Synthesis, crystal structure and 3D energy frameworks of ethyl 2-[5-nitro-2-oxopyridine-1(2H)-yl] acetate: Hirshfeld surface analysis and DFT calculations

Karthik Kumara , Fares Hezam Al-Ostoot ,
Yasser Hussein Eissa Mohammed , Shaukath Ara Khanum ,
Neratur Krishnappagowda Lokanath

PII: S2405-8300(18)30262-3
DOI: https://doi.org/10.1016/j.cdc.2019.100195
Article Number: 100195
Reference: CDC 100195

To appear in: *Chemical Data Collections*

Received date: 15 November 2018
Revised date: 2 February 2019
Accepted date: 5 February 2019

Please cite this article as: Karthik Kumara , Fares Hezam Al-Ostoot , Yasser Hussein Eissa Mohammed , Shaukath Ara Khanum , Neratur Krishnappagowda Lokanath , Synthesis, crystal structure and 3D energy frameworks of ethyl 2-[5-nitro-2-oxopyridine-1(2H)-yl] acetate: Hirshfeld surface analysis and DFT calculations, *Chemical Data Collections* (2019), doi: https://doi.org/10.1016/j.cdc.2019.100195

Synthesis, crystal structure and 3D energy frameworks of ethyl 2-[5-nitro-2-oxopyridine-1(2H)-yl] acetate: Hirshfeld surface analysis and DFT calculations

Karthik Kumara,[a, b] Fares Hezam Al-Ostoot,[c, d] Yasser Hussein Eissa Mohammed,[c, e] Shaukath Ara Khanum [c] and Neratur Krishnappagowda Lokanath [a]*

[a]*Department of Studies in Physics, Manasagangotri, University of Mysore, Mysuru, India.*
[b]*Department of Education in Science and Mathematics, Regional Institute of Education, Mysuru, India.*
[c]*Department of Chemistry, Yuvaraja's College, University of Mysore, Mysuru, India.*
[d]*Department of Biochemistry, Faculty of Education and Science, University of Albaidha, Yemen.*
[e]*Department of Biochemistry, Faculty of Applied Science College, University of Hajjah, Yemen.*

Contact email*:* ***lokanath@physics.uni-mysore.ac.in***

Abstract

Pyridine derivatives with different heterocyclic nucleus have shown potent pharmacological properties as a part from the previously marketed drugs. The title compound, ethyl 2-[5-nitro-2-oxopyridine-1(2H)-yl] acetate has been synthesized, characterized by NMR, mass spectroscopy and the molecular structure was confirmed by single crystal X-ray diffraction studies. The crystal structure is stabilized by C–H···O inter and intramolecular hydrogen bond interactions apart from the cycle stacking and N–O···π interactions. The structure exhibits $R_2^2(8)$ and $R_2^2(10)$ supramolecular architecture. Hirshfeld surface analysis revealed that the O...H (45.0%) interactions has the major contribution to the molecular surface. From the 3D molecular energy frameworks the lattice energy of the compound is found to be -266.2 kJ mol^{-1}. The electronic properties of the compound were quantified using quantum chemical computations by density functional theory calculations. Further, the Mulliken atomic charges were estimated, molecular electrostatic potential map was plotted to identify the chemical reactive sites.

Keywords: Pyridine, X-ray diffraction, N–O···π interactions, energy frameworks, DFT calculations.

Specifications Table

Subject area	Medicinal Chemistry, Spectroscopy, Computational Chemistry, Physical Chemistry, Chemical Crystallography.
Compound	Ethyl 2-[5-nitro-2-oxopyridine-1(2H)-yl] acetate
Data category	Crystallographic data
Data acquisition Format	CIF
Data type	Analyzed

Procedure	To a solution of 4-hydroxypyridine (0.03 mol) in dry acetone (35 ml), anhydrous potassium carbonate (0.044 mol) and ethyl chloroacetate (0.044 mol) were added, then the reaction mixture was refluxed at 70^{o} C for 10 hours to afford phenoxyacetic ethyl ester. The progress of the reaction was monitored by TLC [mobile phase: ethyl acetate/hexane (1:3)]. Finally, the crude product on recrystallization with ethanol afforded the title compound as colorless crystal. Yield (85%). A single crystal of dimension 0.37×0.28×0.24 mm^3 of the title compound was selected and X-ray intensity data were collected at a temperature of 293 K on Rigaku XtaLAB mini diffractometer equipped with an X-ray generator operating at 50 kV and 12 mA, using MoKα radiation of wavelength 0.71073 Å. Data was collected with different settings of φ (0° and 360°), keeping the scan width of 0.5° and exposure time of 4 s.
Data accessibility	**CCDC 1585442:** *URL:*https://www.ccdc.cam.ac.uk/conts/retrieving.html

1. Rationale

The literature survey revealed that aza-heterocycles are more interesting, as they modify the electron distribution inside the scaffold which leads to alter the physical and chemical properties of the compounds [1]. In addition to modification of the scaffold reactivity towards metabolic pathways, they also increases its capacity to cross biological barriers. Among the nitrogen containing six-member heterocyclic compounds, the pyridine structure is often found in naturally occurring bio-active compounds such as alkaloids [2]. Pyridine is one of the most prevalent heterocyclic compound in nature. Pyridine substitutes are most utilized as a part of

pharmaceutics as nicotinamides and nicotinic acid derivatives. The different therapeutic capability of pyridine derivatives has been accounted for the treatment of assorted cancers of diverse cells, by focusing on angiogenesis [3], apoptosis and by restricting a most of the tumor promoting factors like focal adhesion kinase (FAK), cyclin-dependent kinase (CDK) and topoisomerase II [4, 5]. Also antiproliferative and apoptogenic properties against Dalton's lymphoma was reported [6]. Pyridine derivatives exhibited various types of biological activities such as antimicrobial [7, 8] antimycobacterial, analgesic antiparkinsonian, anticonvulsant [9], antitumoral [10], cytotoxic [11], antimalarial [12], antidiabetic [13], pesticidal [14], inhibitory and receptor antagonists [15]. Pyridine derivatives also have shown anti-HIV, anticancer and anti-inflammatory activities [16]. In view of their broad spectrum of biological properties, and as a part of our ongoing work on synthesis and characterization of pyridine derivatives [17, 18] the title compound was synthesized. And the compound was spectroscopically characterized, finally the three dimensional structure was affirmed by single crystal X-ray diffraction studies. An investigation of close intermolecular contacts between the molecules via Hirshfeld surface analysis is also performed in order to quantify the interactions within the crystal structure. Further, the 3D energy frameworks calculations have been carried out to compute different interaction energies. Density functional theory calculations were also performed to shed light on electronic and chemical properties of the compound.

2. Experimental procedure

2.1 Materials and methods

All the chemicals were purchased from Sigma Aldrich chemical company and used without further purification. Melting point was determined using the Chemi Line CL725 Micro Controller based melting point apparatus with a digital thermometer. Compound purity was confirmed by TLC on 0.25 mm silica gel plates (Merck 60 F_{254}) using solvent system hexane:

ethyl acetate (3:1). The NMR spectrum (^{1}H and ^{13}C) was recorded on a VNMRS-400 MHz Agilent-NMR spectrophotometer using DMSO solvent, mass spectrum was obtained with a VG70-70H spectrophotometer. Elemental analysis results are within ±0.5% of the calculated value.

2.2 Synthesis of ethyl 2-(5-nitro-pyridine-2-yloxy) acetate (3):

To a solution of 4-hydroxypyridine (**1**, 0.03 mol) in dry acetone (35 ml), anhydrous potassium carbonate (6.4 g, 0.044 mol) and ethyl chloroacetate (**2**, 0.044 mol) were added, then the reaction mixture was refluxed at 70 ^{o} C for 10 hours to afford phenoxyacetic ethyl ester (**3**). The progress of the reaction was monitored by TLC [mobile phase: ethyl acetate/hexane (1:3)]. After completion of the reaction, the mixture was cooled and the solvent was removed by distillation. The residual mass was triturated with cold water to remove potassium carbonate and extracted with ether (3 × 30 ml). The ether layer was washed with 10% sodium hydroxide solution (3 × 30 ml) followed by water (3 × 30 ml) and then dried over anhydrous sodium sulfate and evaporated to afford compound (**3**) as yellow liquid which slowly solidify [18].

Synthesis of ethyl 2-[5-nitro-2-oxopyridine-1(2H)-yl] acetate (4):

The compound (3) dissolved in ethanol (10 ml) was kept three days for crystallization and was left undisturbed at room temperature to obtain colorless single crystals of ethyl 2-[5-nitro-2-oxopyridine-1(2H)-yl] acetate (4). A schematic diagram for the synthesis of the title compound is shown in **Fig. 1**. The structure of newly synthesized compound was assigned on the basis of NMR, LC-MS spectroscopic data and also by C, H and N elemental analysis. The ^{1}H NMR spectrum (**Fig. 2**) showed disappearance of -OH proton of compound (**1)** and appearance of CH_2, CH_3 protons of the title compound (**3)**. In addition, the mass spectrum (**Fig. 3**) gave significant stable [M+1] peak at 227.51(m/z) which clearly affirmed the formation of the compound (**4)**.

Yield 85%. M.P. 67-69 ^{o} C. ^{1}H NMR (400 MHz, DMSO) δ: 1.18 (t, 3H, CH_3 of ester), 4.13 (q, 2H, CH_2 of ester), 4.82 (s, 2H, CH_2), 6.52 (d, 1H, Ar-H), 8.16 (d, 1H, Ar-H), 9.21 (s, 1H, Ar-H); ^{13}C NMR (100 MHz, DMSO) δ: 13.6 (1C, CH_3) , 59.5 (1C, -CH_2), 75.6 (1C, -CH_2), 117 (1C, Ar-C), 130 (1C, Ar-C) 133 (1C, Ar-C), 143 (1C, Ar-C), 171 (1C, Ar-C), 172.3 (1C, C=O); LC-MS (m/z): 227.50 [M+1]. Anal. Calcd. for $C_9H_{10}N_2O_5$ (226.50): C, 47.79; H, 4.46; N, 12.39 Found: C, 46.60; H, 4.40; N, 12.30%.

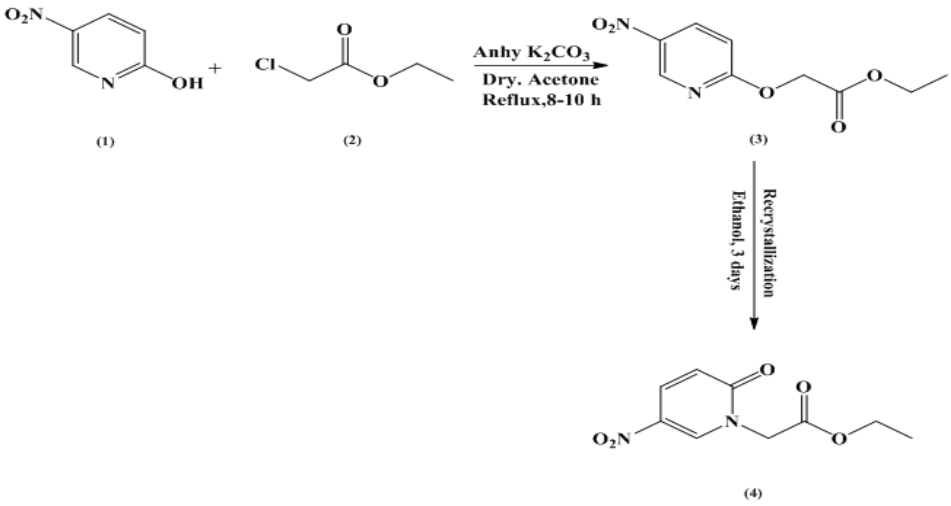

Fig.1: Schematic representation of the synthesis of the title compound.

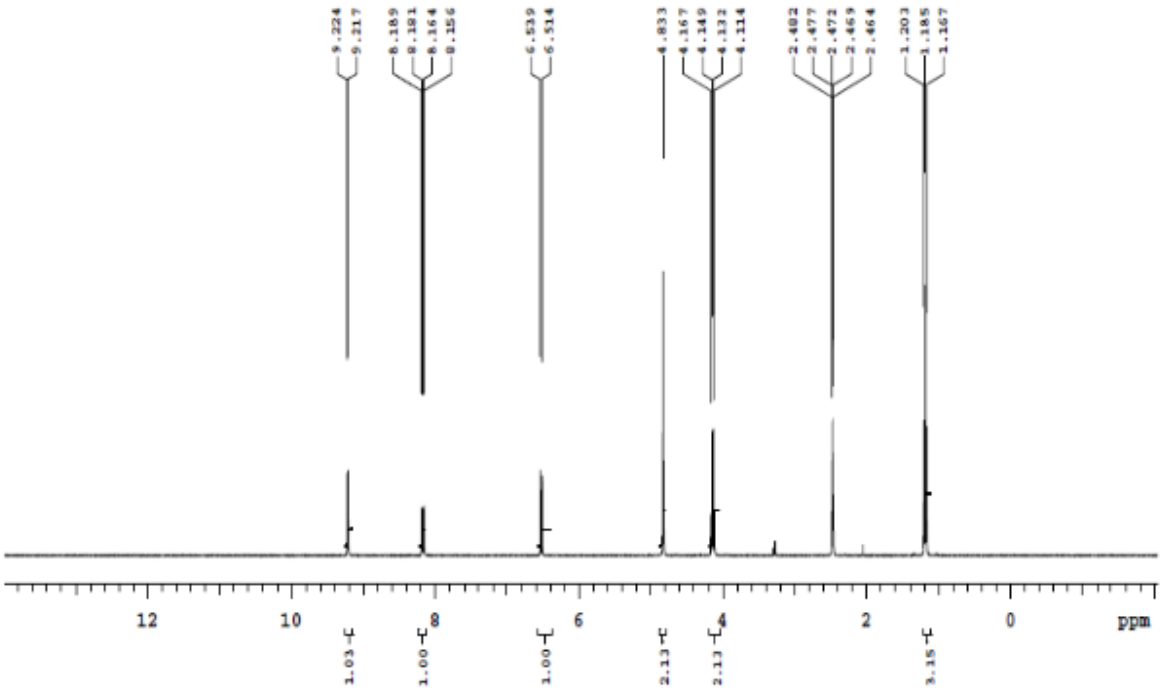

Fig. 2: ^{1}H NMR spectrum of the title compound.

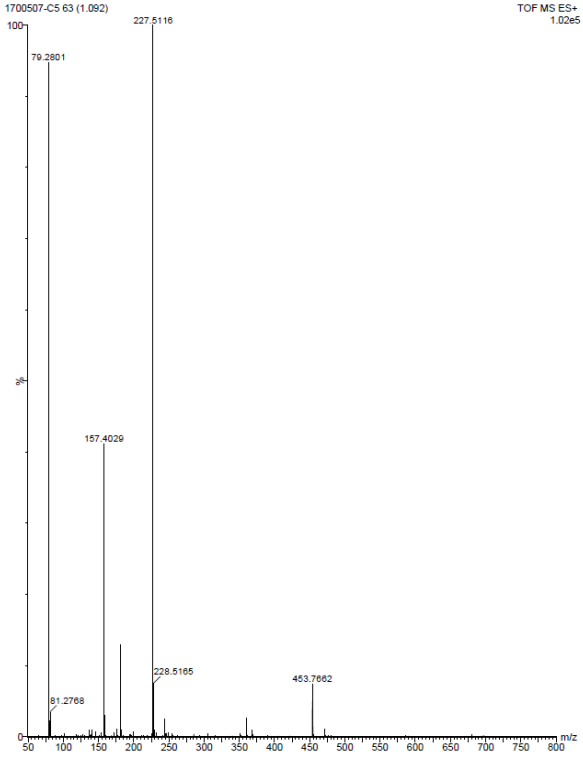

Fig. 3: Mass spectrum of the title compound.

2.3 Crystallographic data collection

A block shaped colourless defect free single crystal of appropriate dimension was chosen for X-ray diffraction studies. X-ray intensity data for the title compound were collected using Rigaku XtaLAB Mini diffractometer with X-ray generator operating at 50 kV, 12 mA and MoK_{α} radiation. Data were collected with χ fixed at 54° and for different settings of φ (0° and 360°), keeping the scan width of 0.5° with exposure time of 4 s and the sample to detector distance was fixed to 50 mm. The title compound ($C_9H_{10}N_2O_5$) was crystallized in the triclinic crystal system, in $P\overline{1}$ space group. The complete intensity data sets were processed using *CRYSTAL CLEAR* [19]. The crystal structure was solved by direct method and refined by full-matrix least squares method on F^2 using *SHELXS* and *SHELXL* program [20]. All the non-hydrogen atoms were refined anisotropically and the hydrogen atoms were positioned geometrically, with C-H = 0.93-0.97 Å and the final refinement using a riding model with U_{iso}(H) = 1.2 U_{eq}(C), U_{iso}(H) = 1.5 U_{eq}(C_{methyl}). After several cycles of refinement, the final difference Fourier map showed peaks of no chemical significance and the residual is saturated to 0.0677. The geometrical calculations were carried out using the program *PLATON* [21]. The molecular and packing diagrams were generated using the software *MERCURY* [22].

2.4 Density functional theory, Hirshfeld surface analysis and 3D energy frameworks

The theoretical quantum chemical computations were carried out using density functional theory (DFT) performed with *Gaussian16* package [23]. The structural coordinates of the compounds were optimized with B3LYP hybrid functional and 6-311G+(d,p) level basis set [24-28] in gas phase. Further, the electronic properties, molecular orbital energies and Mulliken atomic charges of the compound were computed. The molecular electrostatic potential (MEP) map was plotted and molecular orbitals were visualized using *Gaussview* 6.0.8 [29] without any constraints on the geometry. The Hirshfeld surface analysis was carried out using *CrystalExplorer* 17.5 [30] program to quantify and visualize different molecular interactions. The interaction energies between the molecules in the crystalline environment were calculated from the monomer wave functions at B3LYP/6-31G(d,p) for the 3D energy framework analysis.

3. Results and discussion

3.1 Single crystal X-ray diffraction studies

Single crystal X-ray diffraction analysis revealed that the title compound ($C_9H_{10}N_2O_5$) crystallizes in the triclinic crystal system in $P\bar{1}$space group. The crystallographic data is deposited at Cambridge Crystallographic Data Center with data access number CCDC 1585442. The ORTEP of the molecule with thermal displacement ellipsoids drawn at 50% probability level is shown in **Fig. 4**. The complete details of the crystal data and structure refinement statistics are given in **Table 1**.

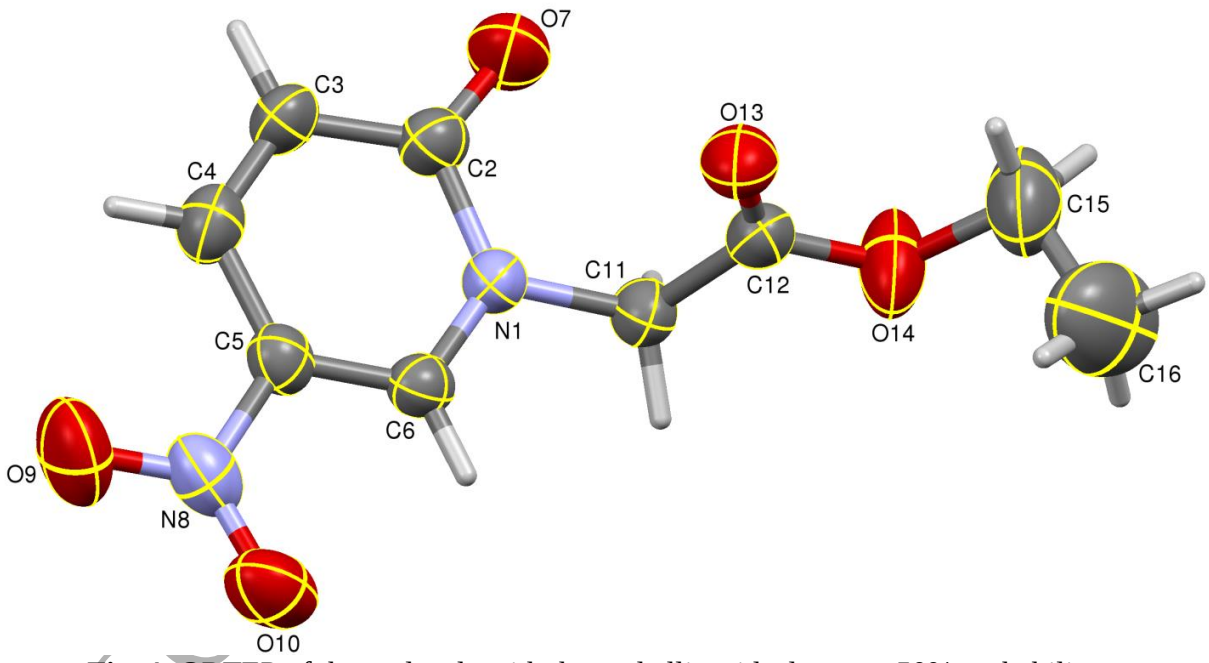

Fig. 4: ORTEP of the molecule with thermal ellipsoids drawn at 50% probability.

Table 1: Crystal data and structure refinement details.

Parameter	value
CCDC deposit No.	CCDC 1585442
Empirical formula	$C_9H_{10}N_2O_5$
Formula weight	226.19
Temperature	293 K
Wavelength	0.71073 Å
Crystal system, space group	Triclinic, $P\bar{1}$
Unit cell dimensions	a = 4.9970(5) Å b = 10.4289(5) Å c = 11.3781(5) Å α = 64.81(4)^o β = 77.94(6)^o γ = 80.05(6)^o
Volume	522.4(2) Å^3
Z	2
Density(calculated)	1.438 Mg m^{-3}
Absorption coefficient	0.119 mm $^{-1}$
F_{000}	236
Crystal size	0.37 × 0.28 × 0.24 mm^3
θ range for data collection	3.50^o to 27.43^o
Index ranges	−6 ≤ h ≤ 6 −13 ≤ k ≤ 12 −14 ≤ l ≤ 9
Reflections collected	3053
Independent reflections	2329 [R_{int} = 0.0452]
Absorption correction	multi-scan
Refinement method	Full matrix least-squares on F^2
Data / restraints / parameters	2329 / 0 / 146
Goodness-of-fit on F^2	1.048
Final [I > 2σ(I)]	R_1 = 0.0677, wR_2 = 0.1633
R indices (all data)	R_1 = 0.1018, wR_2 = 0.1916
Largest diff. peak and hole	0.453 and -0.332 e Å^{-3}

Single crystal X-ray diffraction studies confirms the molecular structure of the title compound ($C_9H_{10}N_2O_5$). The bond lengths and bond angles are in good agreement with the standard values, and the list of selected bond lengths and bond angles are given in **Table 2** and **Table 3**.

The molecular structure consists of a single six membered nitro-pyridine ring as main core structure with a ethyl acetate chain connected at N1 position of the ring. The observed bond distance of C2-O7 is 1.231(4) Å and C12-O13 is 1.192(4) Å which is evident for the carbonyl form and consistent with the C=O bond. Similarly, the bond distance of C12-O14 is 1.334(4) Å and C15-O14 is 1.466(5) Å which is evident for the C-O bond and are comparable with the standard bond distances [31]. The bond C3-C4 has the bond distance of 1.350(4) Å, which is consistent with the C=C bond. Further, the torsion angle describes the conformation of the molecule, and the list of torsion angles are given in **Table 4**. The pyridine ring [N(1)-C(2)-C(3)-C(4)-C(5)-C(6)] is planar with sigplan value of 0.009. The dihedral angle between the ring plane and the plane of the ethyl acetate chain is 77.89(14)^o indicating the non-planarity of the molecule. The torsion angle value of 76.4(3)^o for C2-N1-C11-C12 confirms the +s*yn-clinal* conformation. The nitro substitution of the ring is in the same plane of the ring as indicated by the torsion angle values of 3.2(5)^o for O9-N8-C5-C4 and 3.8(4)^o for O10-N8-C5-C6. The structure exhibits C–H···O type inter and intramolecular hydrogen bond interactions (**Table 5**).

Table 2. Bond lengths (Å).

Atoms	Bond lengths	
	XRD	DFT
O7-C2	1.231(4)	1.217
O9-N8	1.230(3)	1.226
O10-N8	1.227(4)	1.228
O13-C12	1.192(4)	1.202
O14-C12	1.334(4)	1.338
O14-C15	1.466(5)	1.458
N1-C2	1.411(4)	1.439
N1-C6	1.356(4)	1.349
N1-C11	1.461(3)	1.457
N8-C5	1.449(4)	1.455

C2-C3	1.438(4)	1.449
C3-C4	1.350(4)	1.357
C4-C5	1.412(4)	1.420
C5-C6	1.357(4)	1.366
C11-C12	1.506(4)	1.508
C15-C16	1.420(7)	1.433
Correlation Coefficient (CC)		0.9955

Table 3. Bond angles (^{o}).

Atoms	Bond angles	
	XRD	DFT
C12-O14-C15	118.7(3)	117.1
C2-N1-C6	122.9(2)	123.0
C2-N1-C11	117.6(2)	116.7
C6-N1-C11	119.5(2)	120.1
O9-N8-O10	123.8(3)	124.8
O9-N8-C5	117.2(3)	117.2
O10-N8-C5	119.1(2)	118.0
O7-C2-N1	119.0(3)	119.6
O7-C2-C3	125.9(3)	126.3
N1-C2-C3	115.1(3)	114.1
C2-C3-C4	121.8(3)	122.5
C3-C4-C5	119.6(3)	119.4
N8-C5-C4	121.1(3)	120.9
N8-C5-C6	118.6(3)	118.9
C4-C5-C6	120.2(3)	120.2
N1-C6-C5	120.3(3)	120.8
N1-C11-C12	112.3(2)	111.6
O13-C12-O14	125.3(3)	124.7
O13-C12-C11	126.0(3)	126.0
O14-C12-C11	108.7(2)	109.3
O14-C15-C16	108.1(4)	111.2
Correlation Coefficient (CC)		0.9997

Table 4. Torsion angles (°).

Atoms	Torsion angles	
	XRD	DFT
C15-O14-C12-O13	1.3(5)	0.19
C15-O14-C12-C11	−179.2(3)	-179.18
C12-O14-C15-C16	107.7(4)	86.66
C6-N1-C2-O7	178.5(3)	177.23
C11-N1-C2-O7	−2.1(4)	-2.27
C6-N1-C2-C3	−1.9(4)	-3.12
C11-N1-C2-C3	177.5(3)	178.09
C6-N1-C11-C12	−104.1(3)	-80.83
C2-N1-C6-C5	1.1(4)	2.87
C11-N1-C6-C5	−178.4(3)	-177.68
C2-N1-C11-C12	76.4(3)	94.29
O10-N8-C5-C6	3.8(4)	1.02
O9-N8-C5-C4	3.2(5)	0.75
O9-N8-C5-C6	−175.4(3)	-179.14
O10-N8-C5-C4	−177.6(3)	-179.1
N1-C2-C3-C4	1.4(4)	1.89
O7-C2-C3-C4	−179.0(3)	-178.49
C2-C3-C4-C5	−0.1(5)	-0.44
C3-C4-C5-N8	−179.4(3)	-179.86
C3-C4-C5-C6	−0.9(5)	-0.02
N8-C5-C6-N1	179.0(3)	178.94
C4-C5-C6-N1	0.4(5)	1.17
N1-C11-C12-O13	2.7(4)	9.33
N1-C11-C12-O14	−176.8(3)	-171.66
Correlation Coefficient (CC)		0.9931

Table 5: Geometric parameters for hydrogen bond interactions (Å, °).

D–H...A	D–H	H...A	D...A	D–H...A
C(15)–H(15B)...O(13)*	0.97	2.35	2.745(5)	103
C(3)–H(3)...O(7)^{i}	0.93	2.55	3.481(4)	177
C(6)–H(6)...O(13)^{ii}	0.93	2.51	3.325(4)	146
C(11)–H(11B)...O(13)^{ii}	0.97	2.47	3.397(3)	160
C(16)–H(16B)...O(9)^{iii}	0.96	2.59	3.522(7)	164

*Intra. i: -*x*, 1-*y*, -*z*; ii: 1+*x*, *y*, *z*; iv: -1+*x*, -1+*y*, 1+*z*.

The structure also exhibits the stacking interaction [32-34]; *Cg*(1)···*Cg*(1) (*Cg(1)* is the centroid of the ring N1/C2/C3/C4/C5/C6 with a *Cg*-*Cg* distance of 4.3757(2) Å, α = 0°, β = 39.1°, γ = 39.1°, a perpendicular distance of *Cg*1 (centroid) on itself is 3.3963(1) Å and a symmetry code of 1-*x*, 1-*y*, -*z* with slippage of 2.759 Å. The molecular structure also involves, N–O··π interaction; N(8)–O(10)···*Cg1* with a N–Cg distance of 3.843(3) Å, O···Cg distance of 3.439(2) Å, N–O···Cg angle of 99.77(2)°, and with a symmetry code 1+*x*, *y*, *z*. **Fig. 5** showing the packing of the molecules when viewed down the *a*-axis, the dotted lines indicating the hydrogen bond interactions. The bridging of molecules through C–H···O intermolecular hydrogen bond interactions between carbonyl oxygen, oxygen of nitro group and the hydrogen of phenyl ring form $R_2^2(8)$ and $R_2^2(10)$ supramolecular ring motifs [35-36] and are shown in **Fig. 6**. The molecular stacking along the *a*-axis through N–O··· π interactions is shown in **Fig. 7.**

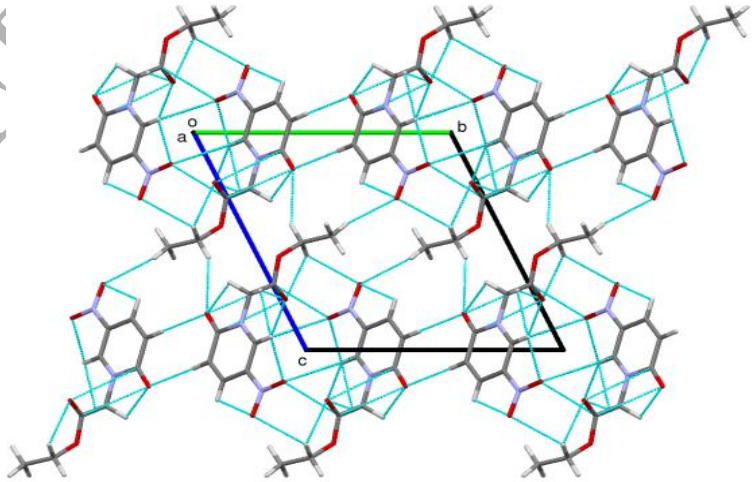

Fig. 5: The packing of the molecules when viewed down the *a*-axis. The dotted lines indicating the hydrogen bond interactions.

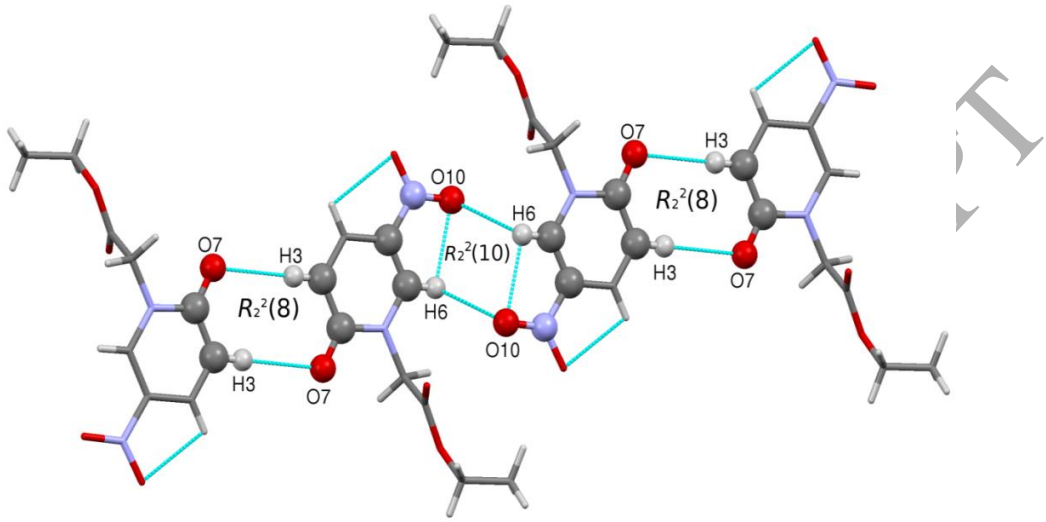

Fig. 6: $R_2^{\,2}$ (8) and $R_2^{\,2}$ (10) supramolecular ring motif formation through C–H···O intermolecular hydrogen bond interactions.

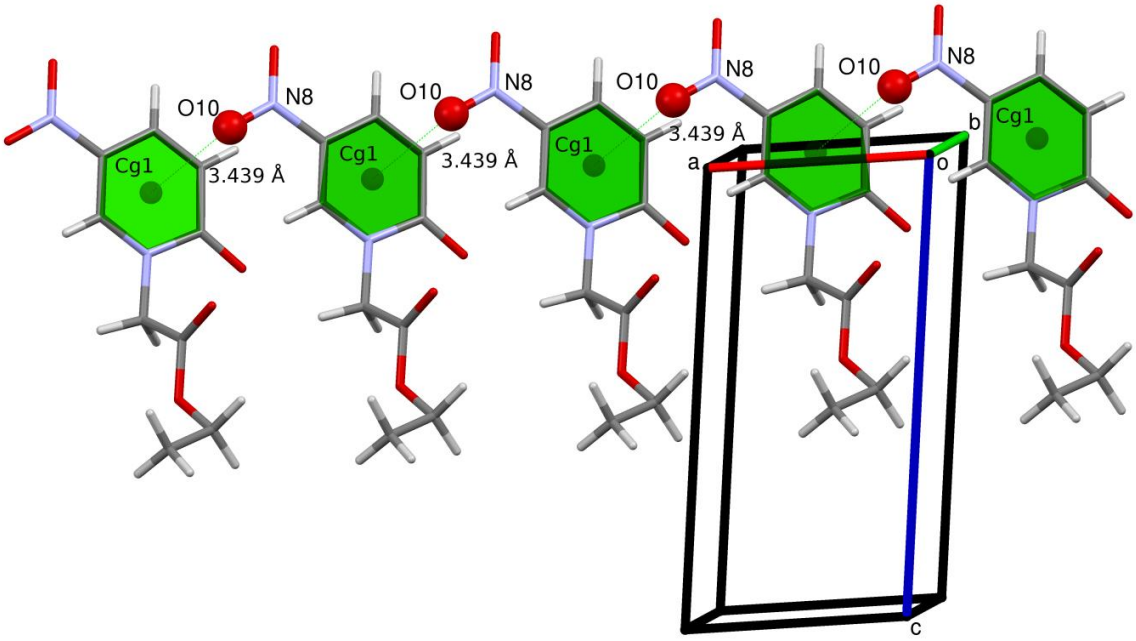

Fig. 7: N–O··· $\boldsymbol{\pi}$ stacking interactions along the *a*-axis.

3.2 Hirshfeld surface studies

Hirshfeld surface analysis helps to understand the molecular interactions in crystalline environment and the graphical visualization of the molecular surface. Analysis and calculations of the Hirshfeld surface were carried out by uploading the crystallographic information file to the *CrystalExplorer* 17.5 software. The d_{norm} plots were mapped with color scale in between −0.182 au (blue) to 1.195 au (red) respectively. The expanded 2D fingerprint plots [37-38] were displayed in the range of 0.6 - 2.8 Å view with the d_e and d_i distance scales displayed on the graph axes. Here d_e and d_i are the distances to the nearest nuclei outside and inside the surface from the Hirshfeld surface respectively. The calculated volume inside the Hirshfeld surface is 255.55 $Å^3$ in the area of 254.23 $Å^2$.

The analysis of 2D fingerprint plot gives the quantitative contributions of molecular contacts to the total Hirshfeld surface. The O...H (45.0%) contacts has maximum and C...N (0.9%) has minimum contributions. Similarly, the H...H (31.1%), C...O (7.7%), C...H (5.6%), O...O (4.1%), O...N (2.2%), N...H (1.8%) and C...C (1.7%) contacts also contribute to the total area of the surface as shown in **Fig. 8.** These contacts are highlighted on the molecular Hirshfeld surface using conventional mapping of d_{norm}, electrostatic potential, shape index, curvedness and fragment patches as shown in the **Fig. 9.** The colored regions on the molecular surfaces can be used to analyze the different properties of the molecular surface. The regions with red and blue color on the d_{norm} represent the shorter and longer inter contacts, the white color indicates the contacts around the van der Waals radii. The electrostatic potential map is plotted on Hirshfeld surface using DFT-B3LYP/6-31G(d,p) hybrid functional. The region with red color represents the negative potential with electrophilic nature and the blue color represents the positive potential with nucleophilic nature. Similarly, the shape index mapped on Hirshfeld surface represents the red triangle concave regions of cycle stacking interactions and the blue triangle convex regions of the ring atoms of the molecule [39-42]. The fragment patches on the molecular surface represents the different molecular interactions.

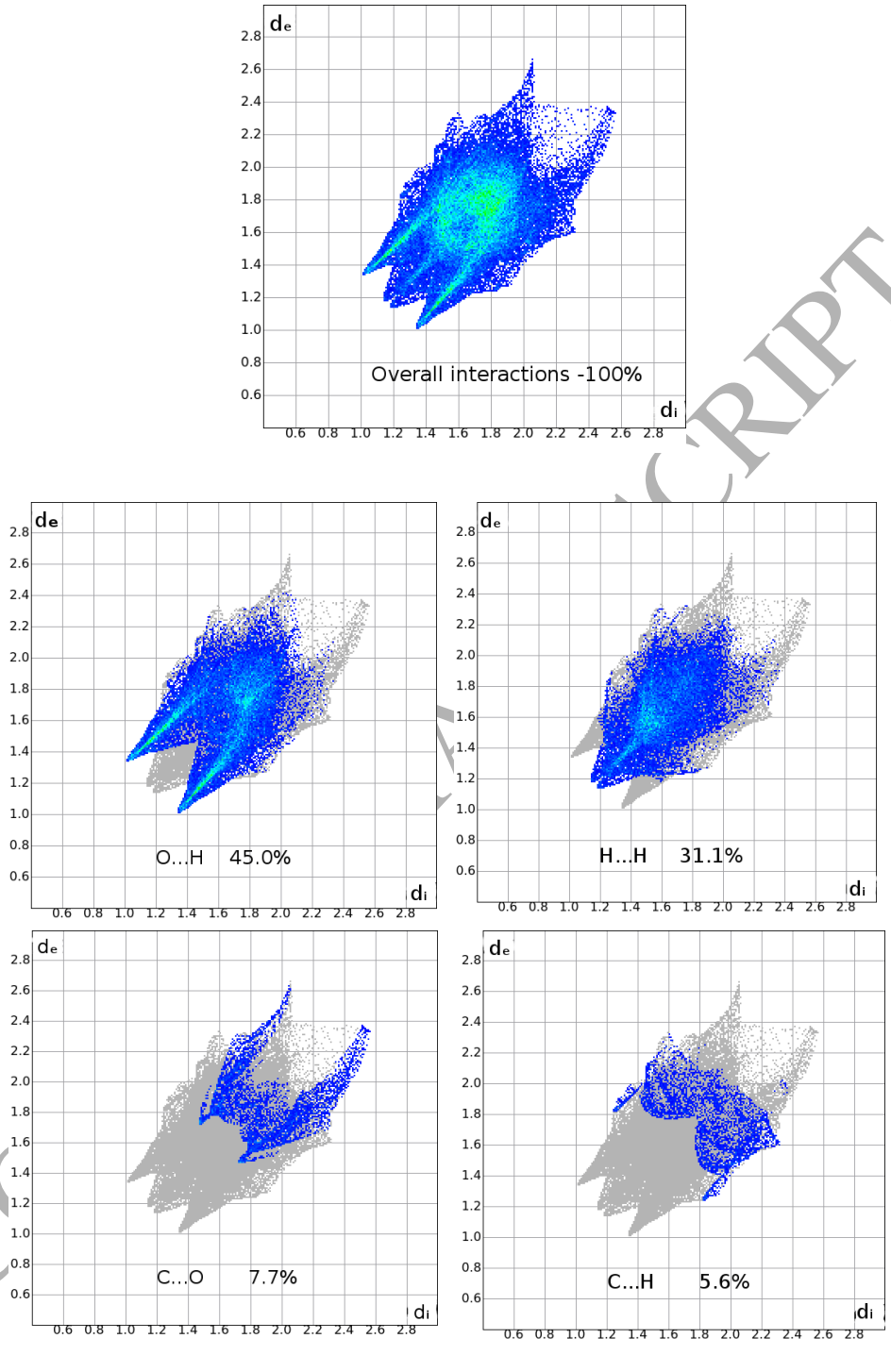

Fig. 8: 2D Fingerprint plots of the title compound showing the individual contribution of each interaction to the total Hirshfeld surface.

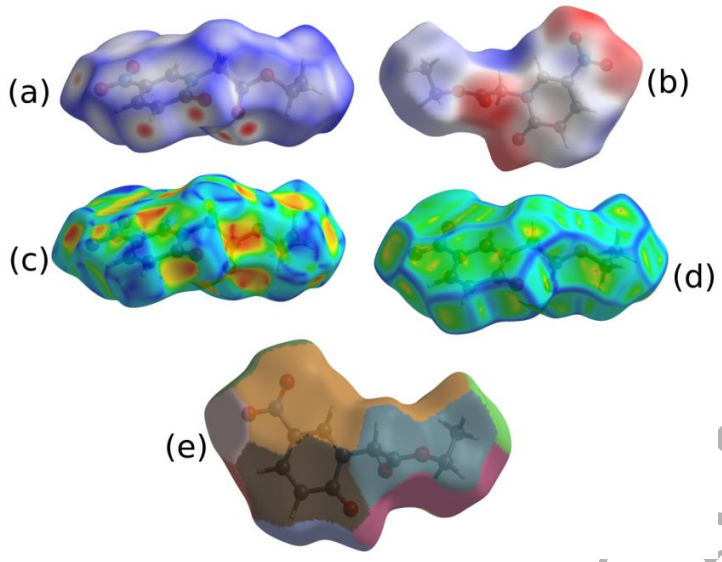

Fig. 9: d_{norm}(a), electrostatic potential (b), shape index (c), curvedness (d) and fragment patches (e) mapped on Hirshfeld surface of the molecule.

3.3 Interaction energy and 3D energy frameworks

The interaction energy between the molecules can be calculated with the most efficient procedure [43-45] using the *CrystalExplorer* 17.5 software. The total interaction energy was calculated by generating the molecular cluster (**Fig. 10**) of radius 3.8 Å around the selected molecule. The energy framework calculations were performed by employing symmetry operations to compute molecular wave functions and to generate electron densities of the cluster of molecules present around the selected molecule using the CE-B3LYP/6-31G(d,p) energy model with scale factors to determine E_{tot} : k_{ele} = 1.057, k_{pol} = 0.740, k_{dis} = 0.871, k_{rep} = 0.618.

Table 6 represents the crystallographic symmetry operations and the corresponding molecular interaction energies (where *R* is the distance between molecular centroids (mean atomic position) in Å and *N* is the number of molecules at that distance, energies are in kJ mol^{-1}). The yellow colored molecule with symmetry operation (*x*, *y*, *z*) located at distance of 5 Å from the centroid of the selected molecule has shown the highest total interaction energy of -42.4 kJ mol^{-1}, whereas the light blue colored molecule with symmetry operation (-*x*, -*y*, -*z*) located at a distance of 12.47 Å from the centroid of the selected molecule has shown the lowest total interaction energy (-1.9 kJ mol^{-1}).

The total interaction energy (-192.5 kJ mol^{-1}) involving the electrostatic (-92.27 kJ mol^{-1}), polarization (-21.978 kJ mol^{-1}), dispersion (-151.72 kJ mol^{-1}) and repulsion (73.23 kJ mol^{-1}) energy terms were evaluated by energy frameworks construction using molecular pair interaction energy calculations. The energy frameworks of the compound were generated for electrostatic, dispersion and total energy terms and represented in terms of different colored cylinders with scale factor (cylinder tube size) 150 and cutoff energy -50 kJ/mol. These cylinders represent the magnitude of the interaction energy between molecular pairs and the strength of the molecular packing along different directions. The molecular cluster with red cylinders represents the electrostatic energy (E_{elec}), green color cylinders represent dispersive energy (E_{dis}) and blue cylinders represents the total interaction energy (**Fig. 11**). The energy framework calculations proved that the dispersion energy dominates over the electrostatic and polarization energies in the crystal environment. The lattice energy for the title compound is found to be -266.2 kJ mol^{-1}.

Table 6: Molecular interaction energies (kJ mol^{-1}) of the cluster of molecules. Each energies should be multiply by the conversion factors k_{ele} = 1.057, k_{pol} = 0.740, k_{dis} = 0.871, k_{rep} = 0.618 to obtain the total energy (E_{tot}).

Molecule color	*N*	Symop	*R* in Å	E_{ele}	E_{pol}	E_{dis}	E_{rep}	E_{tot}
	1	*-x, -y, -z*	8.95	-13.2	-4.3	-19.7	11.9	-26.9
	1	*-x, -y, -z*	4.65	-10.3	-3.3	-27.3	13.8	-28.6
	2	*x, y, z*	5	-22.2	-6.5	-35.8	27.6	-42.4
	2	*x, y, z*	12.51	-3.3	-0.8	-4.4	5.1	-4.7
	1	*-x, -y, -z*	8.28	-20.8	-4.1	-10.4	15.9	-24.3
	1	*-x, -y, -z*	5.66	-21.5	-7.1	-28.3	23.5	-38.1
	1	*-x, -y, -z*	12.47	0.7	-0.2	-4	1.4	-1.9
	2	*x, y, z*	11.71	0.4	-0.6	-5.9	3.5	-3
	1	*-x, -y, -z*	8.02	1.4	-1.6	-17.4	6	-11.1
	1	*-x, -y, -z*	6.86	1.5	-1.2	-21	9.8	-11.5

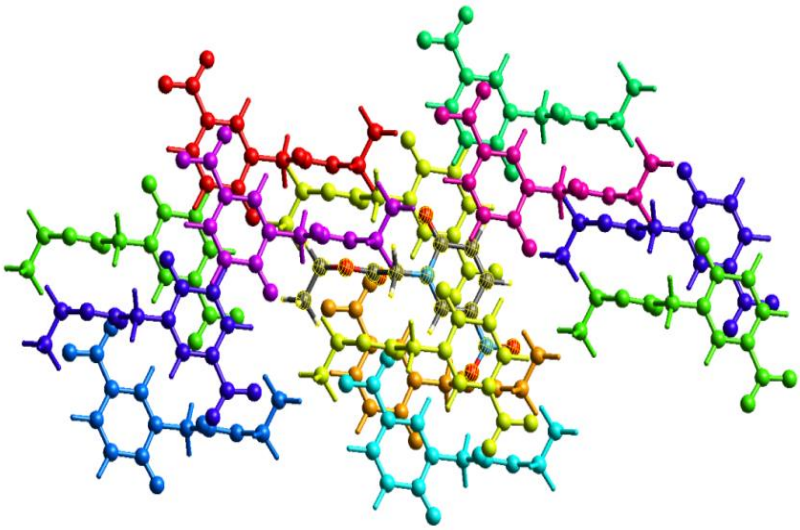

Fig. 10: Molecular interactions between the selected molecule (at the center) and the molecules present in a cluster of radius 3.8 Å.

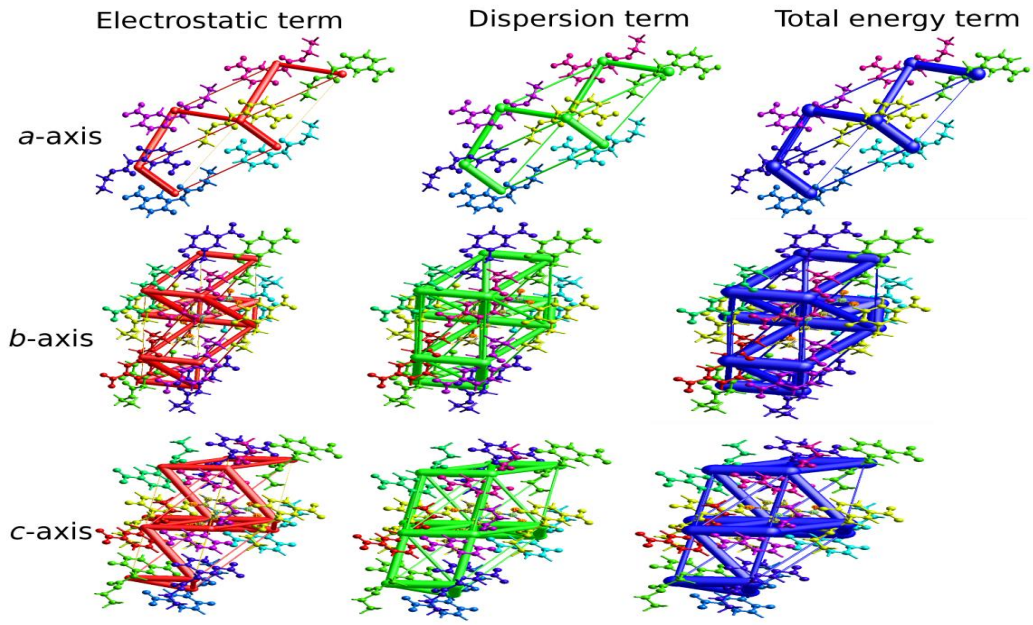

Fig. 11: The energy frameworks of the compound along *a*, *b*, *c*-axes for electrostatic energy, dispersion energy and total energy terms.

3.4 Quantum chemical calculations and frontier molecular orbitals

The quantum chemical calculations, analysis of the frontier molecular orbitals, atomic charges and surface studies play an important role to understand the electronic and chemical properties of the compound. The molecular coordinates of the compound were optimized by DFT calculations using *Gaussian16* software with B3LYP hybrid functional and 6-311G(d,p) basis set in gas phase. The optimized structure of the compound is shown in **Fig. 12**. Theoretically computed structural parameters (bond lengths, bond angles and torsion angles) are in good agreement with the experimental values, which is confirmed by the correlation coefficient between the experimental and the theoretical values (**Table 2, 3**, and **4** respectively).

Further, the energies of the frontier molecular orbitals (HOMO-LUMO), the band gap energy (E gap), the ionization potential (I), the electron affinity (A), the absolute electronegativity (χ), the global hardness (η), the global softness (σ), the global electrophilicity (ω), the chemical potential (μ) and the dipole moment (D) are calculated and tabulated in **Table 7** [46-49] . The HOMO and LUMO energy plot with the band gap energy is shown in **Fig. 13**.

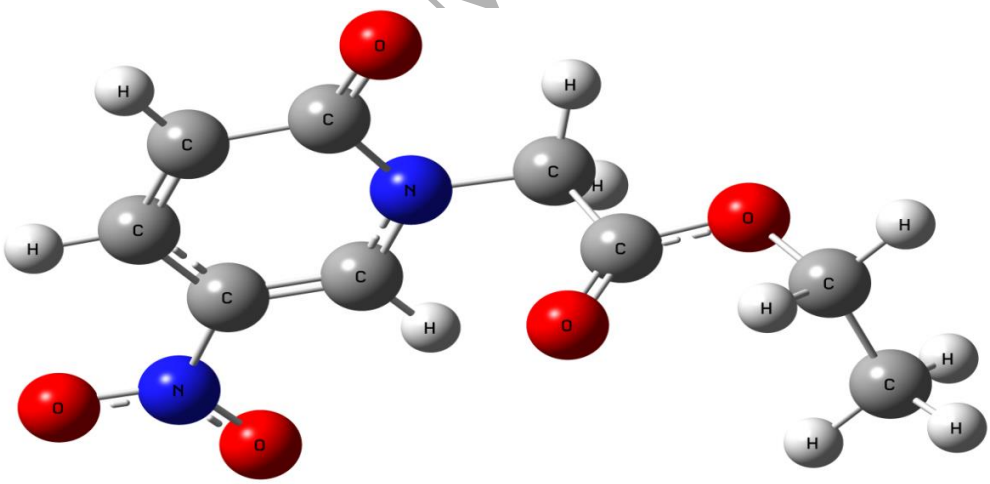

Fig. 12: DFT optimized structure of the title compound.

Table 7: Calculated frontier molecular orbitals and electronic properties of the title compound.

Parameters	Value [B3LYP/6-311G(d,p)] (eV)
E_{HOMO}	-6.9241
E_{LUMO}	-2.5767
ΔE_{gap} (eV)	4.3474
Ionization potential (I)	6.9241
Electron affinity (A)	2.5767
Electronegativity (χ)	4.7504
Chemical hardness (η)	2.1737
Global softness (σ)	0.4600
Electrophilicity (ω)	5.1907
Chemical potential(μ)	-4.7504
Dipole moment (Debye)	4.5473

where, $\chi = (I+A)/2$, $\eta = (I-A)/2$, $\sigma = 1/\eta$ and $\omega = \mu^2/2\eta$

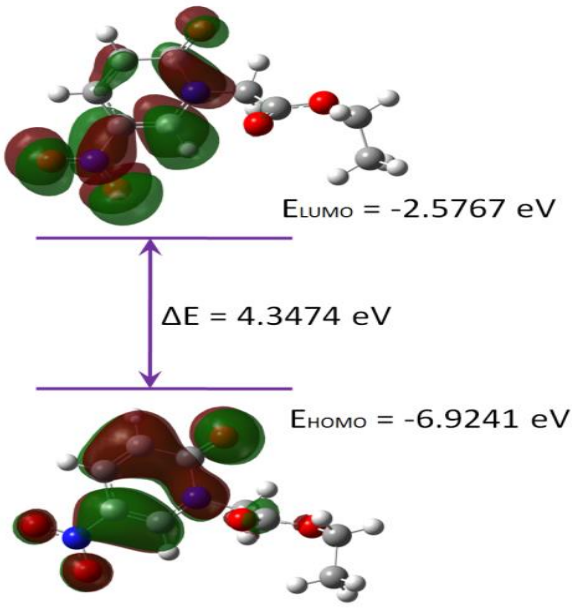

Fig. 13: Frontier molecular orbitals of the title compound.

The Mulliken atomic charges on each atom of the compound have been computed and listed in **Table 8**. The hydrogen atoms attached to the C11 atom have high positive atomic charges when compared to other hydrogen atoms. The oxygen atoms and some carbon atoms have shown

negative charges, and they are readily interacts with the positively charged acceptors. C16 (-0.3121) atom has shown high value of electronegativity due to the electro-positiveness of the three surrounded hydrogen atoms. N1 atom has the highest electronegativity (-0.4167) due to electropositive surrounded atoms.

The molecular electrostatic potential (MEP) map of the compound is generated in the color scale range -4.892 e^{-2} au (deepest red) to +4.892 e^{-2} au (deepest blue) and is shown in **Fig. 14**. The analysis of the MEP surface represents charge distribution on the molecular surface. Based on the colored region on the surface the chemical reactive sites were identified. The positive regions (blue) of MEP represent the electrophilic reactivity, the negative regions (green) related to nucleophilic reactivity of the molecule, and the red regions are related to the electrophilic attack. MEP shows that, the negative regions are concentrated around the oxygen atoms and the blue regions are spread around the hydrogen atoms attached to carbon atoms [50].

Table 8. Mulliken atomic charges of the title compound.

Atom	Charge	Atom	Charge
N1	-0.4167	C11	-0.1456
C2	0.2732	H11A	0.1935
H2	0.1525	H11B	0.1656
C3	-0.0231	C12	0.3906
C4	0.0569	O13	-0.3347
H4	0.1438	O14	-0.3288
C5	-0.2262	C15	-0.0419
H5	0.1327	H15A	0.1327
C6	0.4348	H15B	0.1376
O7	-0.3573	C16	-0.3121
N8	0.1729	H16A	0.1256
O9	-0.2924	H16B	0.1134
O10	-0.2745	H16C	0.1213

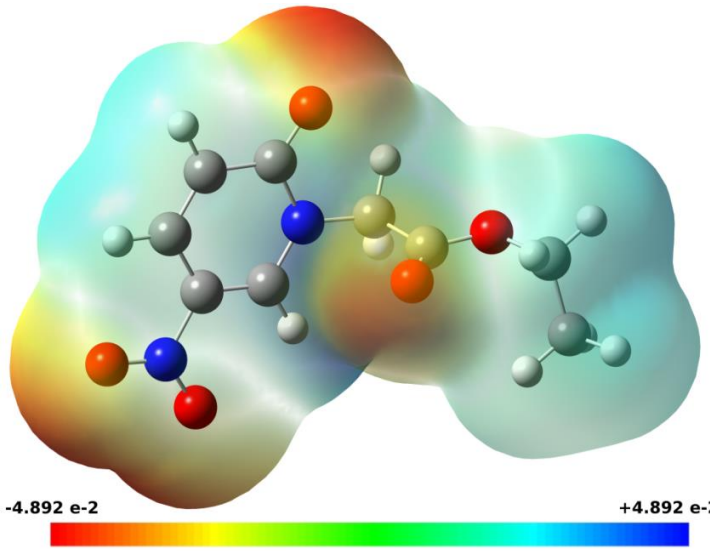

Fig. 14: Molecular electrostatic potential map of the title compound.

4. Conclusions

The title compound $C_9H_{10}N_2O_5$ has been synthesized and the single crystals were grown by the slow evaporation method using ethanol as a solvent. The compound was characterized using the NMR, mass spectroscopy and finally the molecular structure of the compound was confirmed by the single crystal X-ray diffraction studies. The synthesized compound crystallizes in the triclinic crystal system, with $P\bar{1}$ space group. The crystal and molecular structure of the compound is stabilized by inter and intramolecular C–H···O interactions. The structure also exhibits cycle stacking and N–O··π interactions, which contribute to the crystal packing. The molecular Hirshfeld surface analysis and fingerprint plots revealed the nature of molecular interactions and their contribution to the molecular surface, the O...H interaction is found to be the major interactions with highest individual contribution (45.0%). Further, the 3D energy framework revealed that the dispersion energy dominates the electrostatic energy and the lattice energy of the compound is found to be -266.2 kJ mol^{-1}. The structural coordinates were geometrically optimized by DFT calculations using B3LYP hybrid functional with 6-311G(d,p) level basis set. The experimentally obtained structural parameters are well agreed with the theoretically calculated values, confirmed by the correlation coefficient values. The frontier molecular orbital energy calculations revealed that the energy gap between HOMO and LUMO is 4.3474 eV. Further, Mulliken atomic charges and the molecular electrostatic potential surface analysis showed the chemical reactive (electronegative and electropositive) sites of the title compound.

Acknowledgments

Authors are grateful to the Institution of Excellence, DST-PURSE, UPE-projects and National single crystal diffractometer facility, Department of studies in Physics, University of Mysore, Mysuru for providing the X-ray intensity data and computational facilities. Fares Hezam Al-Ostoot is thankful to the government of Yemen and University of Albaidha, Yemen for providing financial assistance under the teacher's fellowship. Yasser Hussein Eissa Mohammed is thankful to the University of Hajjah, Yemen for providing financial assistance under the teacher's fellowship. Shaukath Ara Khanum thankfully acknowledges the financial support provided by VGST, Bangalore, under CISEE Program [Project sanction order: No. VGST/ CISEE /282].

References

[1] Zabiulla, V. Vigneshwaran, A. B. Bushra, G. S. Pavankumar, B. T. Prabhakar, S. A. Khanum, Biomed. Pharmacother. 95 (2017) 419-428.

[2] T. Taniguchi, K. Ogasawara, Org. Lett. 2 (20) (2000) 3193-3195.

[3] P. M. Lukasik, S. Elabar, F. Lam, H. Shao, X. Liu, A. Y. Abbas, S. Wang, Eur. J. Med. Chem. 57 (2012) 311–322.

[4] Y. B. Zhang, W. Liu, Y. S. Yang, X. L. Wang, H. L. Zhu, L. F. Bai, X. Y. Qiu, Med. Chem. Res. 22 (2013) 3193–3203.

[5] J. A. Varela, C. Saa, Chem. Rev. 103 (2003) 3787–3802.

[6] M. Al-Ghorbani, P. Thirusangu, H. D. Gurupadaswamy, V. Girish, H. G. Shamanth Neralagundi, B. T. Prabhakar, S.A. Khanum, Bioorg. Chem. 65 (2016) 73–81.

[7] M. E. Azab, G. A. M. El-hag ali, A. H. F. Abd el-wahab, Acta Pharma. 53 (2003) 213-221.

[8] Y. Cui, Y. Dang, Y. Yang, S. Zhang, R. Ji, Eur. J. Med. Chem. 40 (2005) 209-214.

[9] M. S. Bhatia, A. K. Mulani, P. B. Choudhari, K. B. Ingale, N. M. Bhatia, Int. J. Drug Discov.1 (2009) 1.

[10] A. E. Amr, H. H. Sayeda, M. M. Abdulla, An Int. J. Pharma. Med. Chem. 338 (2005) 433-440.

[11] M. T. Cocco, C. Congiu, V. Lilliuand Onnis, Bioorg. Med. Chem. 15 (2007) 1859-1867.

[12] C. Willemann, R. Grunert, P. J. Bednarski, R. Troschutz, Bioorg. Med. Chem. 17 (2009) 4406-4419.

[13] B. N. Acharya, D. Thavaselvam, M. P.Kaushik, Med. Chem. Res. 17 (2008) 487-94.

[14] R. H. Bahekar, M. R. Jain, P. A. Jadav, V. M. Prajapati, D. N. Patel, A. A. Gupta, A. Sharma, R. Tom, D. Bandyopadhya, H. Modi, P. R. Patel, J. Chem. and Pharma. Sci. 15 (2007) 2115.

[15] T. Singh, S. Sharma, V. K. Srivastava, A. Kumar, Ind. J. Chem. 45B (2006) 1557-1563.

[16] B. Buttelmann, A. Alanine, A. Bourson, R. Gill, M. Heitz, V. Mutel, E. Pinard, G. Trube, R. Wyler, Bioorg. Med. Chem. Lett. 13 (2003) 829-832.

[17] S. M. Kumar, B. C. Manjunath, F. H. Al-Ostoot, M. Jyothi, M. Al-Ghorbani, S. A. Khanum, K. Byrappa, Chem. Data Coll. 15 (2018) 153-160.

[18] Zabiulla, S. Naveen, S. V. Mamatha, J. Mahima, N. S. Lingegowda, N. K. Lokanath, S. A. Khanum, Der Pharma Chemica, 8 (12) (2016) 36-44.

[19] Rigaku, CrystalClear, Rigaku Corporation, Tokyo, Japan (2011).

[20] G. M. Sheldrick, ActaCryst. C 71 (2015) 3–8.

[21] A. L. Spek, ActaCryst. A 46 (1990) c34-c34.

[22] C. F. Macrae, I. J. Bruno, J. A. Chisholm, P. R. Edgington, P. McCabe, E. Pidcock, L. M. Rodriguez, R. Taylor, J. van de Streek, P. A. Wood, J. Appl. Cryst. 41 (2008) 466–470.

[23] M. J. Frisch, G. W. Trucks, H. B. Schlegel, G. E. Scuseria, M. A. Robb, J. R. Cheeseman, G. Scalmani, V. Barone, G. A. Petersson, H. Nakatsuji, X. Li, M. Caricato, A. V. Marenich, J. Bloino, B. G. Janesko, R. Gomperts, B. Mennucci, H. P. Hratchian, J. V. Ortiz, A. F. Izmaylov, J. L. Sonnenberg, D. Williams-Young, F. Ding, F. Lipparini, F. Egidi, J. Goings, B. Peng, A. Petrone, T. Henderson, D. Ranasinghe, V. G. Zakrzewski, J. Gao, N. Rega, G. Zheng, W. Liang, M. Hada, M. Ehara, K. Toyota, R. Fukuda, J. Hasegawa, M. Ishida, T. Nakajima, Y. Honda, O. Kitao, H. Nakai, T. Vreven, K. Throssell, J. A. Montgomery, Jr., J. E. Peralta, F. Ogliaro, M. J. Bearpark, J. J. Heyd, E. N. Brothers, K. N. Kudin, V. N. Staroverov, T. A. Keith, R. Kobayashi, J. Normand, K. Raghavachari, A. P. Rendell, J. C. Burant, S. S. Iyengar, J. Tomasi, M. Cossi, J. M. Millam, M. Klene, C. Adamo, R. Cammi, J. W. Ochterski, R. L. Martin, K. Morokuma, O. Farkas, J. B. Foresman, D. J. Fox, Gaussian 16, Revision B.01, Gaussian, Inc., Wallingford CT, (2016).

[24] C. Lee, W. Yang, R. G. Parr, Phys. Rev. B. 37 (1988) 785.

[25] A.D. Becke, J. Chem. Phys. 96 (1992) 2155-2160.

[26] A. D. Becke, J. Chem. Phys. 98 (1993) 5648-5652.

[27] T. Koopmans, Physica, 1 (1-6) (1934) 104-113.

[28] K. Kumara, A. D. Kumar, K. A. Kumar, N. K. Lokanath, Chem. Data Coll. 13 (2018) 40-59.

[29] R. Dennington, Todd A. Keith, John M. Millam, GaussView, Version 6, Semichem Inc., Shawnee Mission, KS, 2016.

[30] S.K. Wolff, D.J. Grimwood, J.J. McKinnon, M.J. Turner, D. Jayatilaka, M.A. Spackman, CrystalExplorer, University of Western Australia (2012).

[31] H. A. Skinner, Rev. Port. Quim, 29 (39) (1987) 39-46.

[32] K. Kumara, S. Naveen. L. D. Mahadevaswamy, A. K. Kariyappa, N. K. Lokanath, Chem. Data. Coll. 9 (2017) 251-262.

[33] S. K. Seth, D. Sarkar, T. Kar, Cryst. Eng. Comm. 13 (14) (2011) 4528-4535.

[34] C. R. Martinez, B. L. Iverson, Chem. Sci. 3 (7) (2012) 2191-2201.

[35] P. I. Nagy, Int. J. Mol. Sci. 15 (11) (2014) 19562-19633.

[36] J. Bernstein, R. E. Davis, L. Shimoni, N. L. Chang, Angewandte Chemie Int. Edi. Eng. 34 (15) (1995) 1555-1573.

[37] S. K. Seth, J. Mol. Stru. 1064 (2014) 70-75.

[38] J. J. McKinnon, D. Jayatilaka, M. A. Spackman, Chem. Com. 37 (2007) 3814-3816.

[39] V. Channabasappa, K. Kumara, N. K. Lokanath, A. K. Kariyappa, Chem. Data Coll. 15 (2018) 134-142.

[40] S. K. Seth, Cryst. Eng. Comm. 15 (2013) 1772–1781 .

[41] V. Kamat, K. Kumara, S. Shaikh, S. Naveen, N. K. Lokanath, V. Revankar, Chem. Data Coll. 17 (2018) 251-262.

[42] M. A. Spackman, J. J. McKinnon, D. Jayatilaka, Cryst. Eng. Comm. 10 (4) (2008) 377-388.

[43] M. W. Shi, S. P. Thomas, G. A. Koutsantonis, M. A. Spackman, Cryst. Growth Des, 15

(12) (2015) 5892-5900.

[44] U. M. Sumaya, J. Karuna Karan, K. Biruntha, A. K. Mohana Krishnan, G. Usha, Acta Crystallogr. A: Crystallogr. Comm. 74 (7) (2018) 939-943.

[45] C. F. Mackenzie, P. R. Spackman, D. Jayatilaka, M. A. Spackman, IUCr. J. 4(5) (2017) 575-587.

[46] S. Xavier, S. Periandy , S. Ramalingam , Spectrochim. Acta Part A: Mol, Bio. Spect. 137 (2015) 306–320 .

[47] I. Warad , F. F. Awwadi , M. Daqqa , A. Al Ali , T.S. Ababneh , T. M. AlShboul, M. J. Taghreed , F. Al-Rimawi , T. B. Hadda, Y. N. Mabkhot, J. Photochem. Photobio. B: Bio 171 (2017) 9–19 .

[48] Y. X. Sun , Q. L. Hao , Z. X. Yu , W. X. Wei , L. D. Lu , X. Wang, Mol. Phys. 107 (3) (2009) 223–235.

[49] K. Kumara, A. D. Kumar, S. Naveen, K. A. Kumar, N. K. Lokanath, J. Mol. Stru. 1161 (2018) 285-298.

[50] P. Politzer, D. G. Truhlar, Springer Science and Business Media, (2013).

Graphical abstract: